AIAA JOURNAL
Vol. 47, No. 5, May 2009

Concise Airfoil Representation via Case-Based Knowledge Capture

András Sóbester*
University of Southampton, Southampton, England SO17 1BJ, United Kingdom

DOI: 10.2514/1.40119

The cost of exploring a k-dimensional design space at a sampling density n is of the order n^k. In view of this "curse of dimensionality," the paper explores the possibility of reducing the dimensionality of parametric airfoil definitions to as low as one, to minimize their cost impact on full-airframe conceptual design studies. A formulation based on nonuniform rational B-splines is introduced in which the parametric airfoil is constructed in a reduced-dimensionality space defined in terms of a small number of basis geometries. These bases are airfoils themselves, selected to represent key features of their class; we use them as learning cases or case-based representations of our knowledge of what makes a nonuniform rational B-splines curve an airfoil: moreover, an airfoil belonging to a certain class. This study focuses on supercritical sections, but the template presented here can also be applied to other types of airfoils and, indeed, to other classes of curves and surfaces.

Nomenclature

$\mathbf{A}$	=	matrix containing the parameters that define the airfoil
$\bar{\mathbf{A}}$	=	$\mathbf{A}$ with some degrees of freedom constrained
B	=	vector of base airfoils
c_d	=	airfoil drag coefficient
c_l	=	airfoil lift coefficient
d	=	distance metric defined on the space of airfoils
$\mathcal{F}$	=	airframe design objective functional
G	=	airframe geometry
k	=	number of design variables
M_∞	=	freestream Mach number
$N_{i,p}$	=	ith basis function of degree p
n	=	number of levels in a full-factorial sampling plan
p	=	degree of B-spline basis function
T	=	vector of nonuniform rational B-splines knots
t	=	B-spline parameter
t/c	=	airfoil thickness-to-chord ratio
t_i	=	nonuniform rational B-splines knot
v_i	=	airframe geometry design variables
w	=	nonuniform rational B-spline basis function weight
x_i^u, x_i^l	=	abscissa of the ith upper- and lower-surface control points
y_i^u, y_i^l	=	ordinate of the ith upper- and lower-surface control points
α, α_i	=	parametric airfoil design variable(s)
Ω	=	pair of two nonuniform rational B-spline curves
ω	=	target or base airfoil

I. Introduction

THE first station on the journey of an airframe design from clean sheet to final product is the *exploration* exercise known as *conceptual design*. This is a global search, as the design space is at its broadest at this stage; ideally, the geometry definition should be flexible enough to cover a diverse spread of shapes and layouts.

The cost of this flexibility is usually a relatively high number of design variables. This, in turn, leads to a large number of candidate designs for which the merits need to be examined if we are to explore this multivariable design space thoroughly. Although the analysis that yields these conceptual-level merit function values (weight, drag for a specified lift value, etc.) is generally of the low-cost variety, it is still surprisingly easy to run out of any reasonable computing time budget, unless we are as economical as possible with the parameterization of the geometry.

The reason is a phenomenon sometimes referred to as the "curse of dimensionality": n^k designs are needed to explore a k variable space at n levels. This means that even if we merely aim to sample the merit functions at the vertices of the design space [that is, each design variable can only take its extreme values ($n = 2$), a somewhat unsatisfactory observation density], the addition of every new variable doubles the number of required merit function evaluations. If we add a third level to each variable and consider a parametric airframe geometry defined by, say, $k = 20$ parameters [a not unreasonable (if anything, conservative) number in conceptual design], the number of conceivable designs will be $3^{20} \sim 3.5 \times 10^9$. A single additional design variable would now add an *extra order of magnitude* to the size of the design space ($3^{21} \sim 10^{10}$).

Of course, it would be impossible to visit all these designs, and shortcuts are possible. Instead of the full-factorial sample considered previously, more sparse, but still space-filling, sampling plans could be considered (e.g., a Latin hypercube [1]). Evolutionary algorithms and multistart local optimizers are further alternatives when such vast design spaces have to be explored. However, none of this changes the fundamental fact that the expansion of the design space with increasing k will be $\mathcal{O}(n^k)$, and this ought to be among any conceptual designer's foremost concerns.

Clearly, reducing k has the inevitable drawback of restricting the flexibility of the geometry and, in some cases, this may not be an option. Here, we concentrate on the case when, for the reasons outlined previously, we simply *must* minimize k and we are prepared for considerable sacrifices on the flexibility front.

More specifically, we look at the parsimonious parameterization of airfoil sections. These lie at the heart of the definition of all lifting-surface-type elements of an airframe geometry, and together they therefore usually account for a significant fraction of the dimensionality of any parametric airframe definition. Luckily, the flexibility standards expected of airfoil shapes are not quite as high as in the case of the overall airframe, and this opens the door toward attempts at reducing the dimensionality of their parameterization. In what follows, we put forward a formulation for the conceptual-level parametric description of transonic (supercritical) airfoils, though the process is adaptable to other classes of airfoils.

Of course, parametric airfoils go back a very long way into the history of aviation and thus the literature behind them is considerable. It is therefore important to place the present work in the

Received 29 July 2008; revision received 1 February 2009; accepted for publication 22 February 2009.

*Lecturer, Computational Engineering and Design Group. Member AIAA.

context of what is already available to the engineer; we do this next by way of sketching out a short taxonomy of some existing approaches.

II. Taxonomy of Parametric Airfoils

Numerous airfoil geometry definition schemes have been proposed over the first century of flight, and many different criteria could be used to arrange these into a taxonomy. Here, we choose to simply position them along a continuum of design-variable scopes. In other words, we classify them according to the geometrical extent (in terms of the overall size of the airfoil) of the influence of any particular design variable, as this criterion feels the most germane when it comes to clarifying the place of our proposed scheme in the rather broad context of airfoil description methodology.

Consider the extremes of this scale. If a computational fluid dynamics mesh is generated around a putative airfoil, one could designate the coordinates of the mesh points falling onto the airfoil surface as design variables. Sometimes combined with a related mapping of the rest of the mesh, as well as a smoothness constraint designed to prevent the emergence of jagged airfoils, this is a highly successful scheme when a local improvement is sought in relation to the starting point of the design process. The search can be particularly efficient when adjoint gradients are available at a computational cost that is independent of problem dimensionality. A classic example is the control-theory-based formulation of Jameson [2]. Clearly, in this case, the influence of a design variable is restricted to the immediate vicinity of its corresponding mesh point.

Staying with Jameson's [2] work, one can also find here an example of the opposite end of the scale, in which a design parameter's scope is the entire airfoil. In [3], he describes the solution of the potential flow equations over an airfoil, which results from a circle, via a complex conformal mapping (a mapping, which is, incidentally, also applied to the mesh). A very similar example is that of the well-known Jukowski airfoil; in both cases, the impact of changes to the coordinates of the circle being mapped can be seen across the entire airfoil.

All other methods populate the span between these two extremes. Indeed, some can take up different locations along this continuum, depending on how the designer chooses to implement them. Certain formulations are naturally suited to variable resolution strategies; these include B-spline or nonuniform rational B-splines (NURBS)-based models, in which the number of free control points determines the scope at any point (see, for example, [4]). Similarly, the bump functions, introduced by Hicks and Henne [5] at the dawn of the computer-aided design age, can be added to the baseline airfoil scaled to the entire chord or, more locally, to a limited part thereof (see [6] for an 18-variable example). Another way of controlling the scope of the Hicks–Henne parameterization method is to restrict the range of permitted chordwise movement of the peak of the bump (the base of the bump rests on the full chord).

Also, to some extent, variable in scope is the scheme described recently by Kulfan [7]. At the heart of her airfoil description lies a generic template containing a square-root term (to ensure a round leading edge) and a 1-abscissa/chord term to close the trailing edge (with another term specifying a finite trailing-edge thickness). The actual parameterization is encapsulated by a shape-function term with variable flexibility. At its stiffest, the shape function can depend on a single variable; in this case, we can control the nose radius on both the lower and upper surfaces at the same time. It is also possible to set up a one-variable shape function to control the boat-tail angle. Both of these choices place us about halfway down the scope continuum, as the impact of any variable value changes affects either the fore or the aft section of the airfoil. More flexible shape functions can come, for example, in the form of a Bernstein-polynomial partition of unity, which gives increasingly finer and, in some sense, more localized control of the shape (as an illustration of the flexibility of the shape function, [7] includes eighth-order Bernstein-polynomial approximations of the RAE2822 airfoil, which take the approximation errors well below wind-tunnel model tolerances).

Let us now consider a few examples of formulations with more specific places on the parameter-scope scale. Lépine et al. [8] and Painchaud-Ouellet et al. [9] use NURBS curves to define their airfoils, in which the coordinates and the weights of the control points are the design variables. The significant impact of each is, of course, restricted to the vicinity of the relevant control point, and therefore this scheme is close to the local end of the scope scale.

Sixth-order polynomials form the basis of the PARSEC formulation [10]. Each of the 11 design variables is connected to a very specific feature of the airfoil: leading-edge radius, upper and lower crest locations, curvatures at the crests, trailing-edge ordinates, thickness, tail direction, and wedge angle. This is therefore also fairly near to the local end of the scale; each variable affects a well-defined part of the airfoil.

The scopes of the parameters of the formulations based on Ferguson's cubics and B-splines, presented in [11], are based on a similar philosophy. They are slightly more global in scope though, simply by virtue of there being fewer of them (six or seven, depending on whether the trailing edge is sharp or finite).

Near the global end, we find the classic 4-digit NACA foils. The variables here refer to specific features of the airfoil (maximum thickness and its location and maximum camber), but each of these refers to both the upper and the lower surfaces of the airfoil, and thus any change in any of the design variables has some impact on every point. Also, at the global end, we find the orthogonal basis functions of Robinson and Keane [12]. These functions represent features extracted from the NASA Phase 2 supercritical airfoils (described by Harris [13]), and the variables, which are the relative weights of these bases and the thickness-to-chord ratio, affect the shape of the entire airfoil.

We made the point earlier that many other classifications are possible. Equally, one could draw up a large number of different criteria that a parametric airfoil should be required to satisfy (see, for example, the introduction of [7] for a set of eight such desirable features). The work presented here was driven by our own wish list, resulting from the desire to conduct airframe conceptual design in a multidisciplinary design optimization (MDO) environment comprising CAD engines, geometry-based conceptual design tools, and a variety of numerical analysis packages (both standalone and CAD-integrated). The methodology described in this paper was thus conceived as an answer to the following requirements, listed in decreasing order of importance:

1) Conciseness is paramount. Minimizing the problem dimensionality k is the overriding objective, accepting losses in terms of flexibility. This means exploring the possibility of reducing the number of design variables to as low as one, placing the parametric airfoil we seek at the global extreme of the classification discussed previously.

2) NURBS have become the standard formulation for geometry representation in most types of MDO-related software, from CAD through meshing tools to analysis codes. Although workarounds exist for transferring non-B-spline-based geometries into such tools, these processes are rarely error-free. Therefore, we postulate that the representation must be NURBS-based.

3) To minimize the number of wasted automated analysis runs, the entire design space should be feasible. In other words, any combination of design-variable values should produce airfoil-like shapes.

4) The primary area of application is the design of transonic wings, and the parametric airfoil should therefore have the ability to take up supercritical shapes.

5) Design is generally performed at increasing levels of detail. Therefore, multiple levels of flexibility should be built into the same parametric airfoil description.

The fundamental challenge posed by these criteria is how one describes a shape as complex as a supercritical airfoil with a very small number of parameters. First, the parametric airfoil needs to incorporate the essence of what makes an engineer identify a connected pair of splines as an *airfoil*. Although airfoil descriptions used for local refinement-type design searches can allow shapes with multiple bumps, etc. (under the pressure of the objective function

these are unlikely to appear anyway), at the conceptual level, we cannot afford to stray from the space of airfoil-like shapes. Second, the parametric airfoil must capture as many of the salient features of its class (in this case, the class of supercriticals) as possible; that is, it needs to incorporate the essence of what geometrical features make an airfoil *supercritical*.

This knowledge-capture and representation process can happen on a number of different levels and in a number of different ways. Historically, it has mostly been done through *geometrical reasoning*. Take an example from Kulfan's parametric airfoil [7] discussed earlier: the common square-root term of the generic expression is a representation of what we know about the shape of airfoil leading edges in general; or consider the NACA 4-digit family: they capture the concept of airfoil-likeness in the formulation of the polynomials they are made up of, and therefore they look airfoil-like, whatever values we choose for their parameters.

Here, we adopt a different approach: *case-based reasoning*. That is, we "teach" the parametric formulation the essence of airfoil-likeness and supercriticality through examples that, we know for certain, fulfill both criteria. Fundamentally, this approach builds on the idea of combining useful features of existing airfoils, a school of thought with a rich heritage in airfoil design. The same fundamental principle lies at the heart of all basis or shape-function-type formulations, whether the basis functions are extracted from airfoils (such as those of Hicks and Henne [5] and Robinson and Keane [12]) or are complete airfoils themselves (see [14,15]). Here, we apply the same type of reasoning in a generic NURBS-based context, in a formulation that can be extended readily to other classes of curves and surfaces.

We begin by constructing a generic NURBS-based airfoil (Sec. III), which, through its ability to imitate a range of existing supercritical sections (Sec. IV), will represent the examples (or learning cases). We then select two such imitations, which will serve as the bases of a fully global (as per the taxonomy presented earlier) single-variable parameteric airfoil (Sec. V), and we outline a recipe for using this in a design context (Sec. VI). We then consider incorporating three and four learning cases in our parametric airfoil training process in Sec. VII, followed by conclusions and notes on the possibility of generalizing the preceding to other shapes (Sec. VIII).

III. Pair of Nonuniform Rational B-Splines

Rational B-splines are first mentioned by Versprille [16]. Since then they have become the fundamental building block of most geometry standards and CAD tools, and their use in design has been the subject of much research (see, for example, work reported by Schramm et al. [17] and by Samareh [18]): hence our inclusion of them at the top of the airfoil parameterization scheme criteria list. Here, we shall use a pair of NURBS to define the upper and lower surfaces of an airfoil. Let the series of coordinate pairs (x_i^u, y_i^u) and (x_i^l, y_i^l), where $i = 0, \ldots, 5$, define the *control polygons* of the two curves that form the airfoil and are of the form

$$\mathbf{S}^u(t) = \frac{\sum_{i=0}^{5} N_{i,p}(t)(x_i^u, y_i^u)w_i^u}{\sum_{i=0}^{5} N_{i,p}(t)w_i^u}, \qquad t \in [0, 1] \tag{1}$$

for the upper surface and

$$\mathbf{S}^l(t) = \frac{\sum_{i=0}^{5} N_{i,p}(t)(x_i^l, y_i^l)w_i^l}{\sum_{i=0}^{5} N_{i,p}(t)w_i^l}, \qquad t \in [0, 1] \tag{2}$$

for the lower surface. The two surfaces share the fixed nondecreasing knot vector $T = \{t_0, \ldots, t_{p+6}\}$, which we use to define the B-spline basis functions of degree p (order $p + 1$):

$$N_{i,p}(t) = \frac{t - t_i}{t_{i+p} - t_i} N_{i,p-1}(t) + \frac{t_{i+p+1} - t}{t_{i+p+1} - t_{i+1}} N_{i+1,p-1}(t) \tag{3}$$

Note that this linear combination of lower-order basis functions is defined everywhere, though, as we shall see very shortly, we do not actually need it outside the range defined by the extremities of the knot vector. This recursive formulation (due to Cox [19] and De Boor [20]) can be pictured intuitively as a triangle, for which the apex is the basis function to be calculated, the two basis functions needed for its calculation are right underneath it, and so on. The base of the triangle, which effectively controls the ranges of influence of the control points, is defined as

$$N_{i,0}(t) = \begin{cases} 1 & \text{if } t_i \le t < t_{i+1} \\ 0 & \text{otherwise} \end{cases} \tag{4}$$

For the definition of both the upper and the lower surfaces of the airfoil, we set $p = 2$ and

$$T = \{0, 0, 0, 0.25, 0.5, 0.75, 1, 1, 1\} \tag{5}$$

where the multiplicity of the extreme values indicates that the curve will actually pass through the first and the last control point† [the leading-edge point and the trailing-edge point(s) in our case; more on this shortly]. The reader interested in why this is so and, indeed, in any other detail of the preceding, might find the standard text by Piegl and Tiller [21] edifying.

Let the pair $\Omega(\mathbf{A}) = [\mathbf{S}^u, \mathbf{S}^l]$ thus denote a NURBS aerofoil, where the matrix $\mathbf{A}$ provides an at-a-glance view of all the relevant parameters defining the airfoil (each column corresponds to a pair of control points on either side of the airfoil):

$$\mathbf{A} = \begin{bmatrix} x_0^u & x_1^u & x_2^u & x_3^u & x_4^u & x_5^u \\ y_0^u & y_1^u & y_2^u & y_3^u & y_4^u & y_5^u \\ w_0^u & w_1^u & w_2^u & w_3^u & w_4^u & w_5^u \\ x_0^l & x_1^l & x_2^l & x_3^l & x_4^l & x_5^l \\ y_0^l & y_1^l & y_2^l & y_3^l & y_4^l & y_5^l \\ w_0^l & w_1^l & w_2^l & w_3^l & w_4^l & w_5^l \end{bmatrix} \tag{6}$$

This gives us a total of 36 potential degrees of freedom, a number of which we choose to fix. First, the leading-edge points of both surfaces will always be at (0,0) (see Fig. 1). The chord length will also be fixed (at 1) and so will all the control-point abscissas, with points 0 and 1 being fixed at $x = 0$ and with point 5 (on both sides) always having an abscissa of 1. The remaining control points will be, in terms of their x coordinates, uniformly distributed along the chord. These decisions halve the number of degrees of freedom contained in $\mathbf{A}$ and we shall, in what follows, refer to this constrained form of the variable definition matrix as

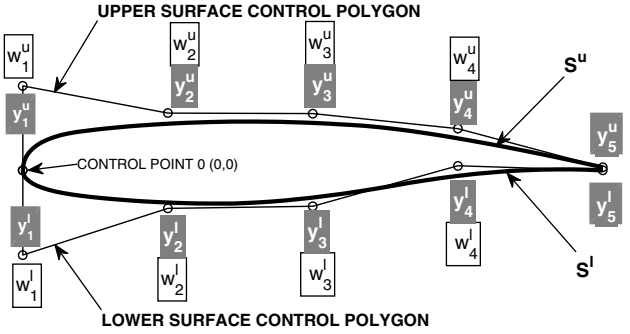

Fig. 1 Control-point weights (framed) and ordinates (on gray background) through which we determine the shape of the NURBS-based airfoil.

†This mirrors the formulation used, for example, by the ubiquitous openGL graphics library. Other similar libraries may differ slightly; for example, readers wishing to implement the scheme described here in an open NURBS-based package should define the knot vector as $T = \{0, 0, 0.25, 0.5, 0.75, 1, 1\}$.

$$\bar{\mathbf{A}} = \begin{bmatrix} 0 & 0 & 0.25 & 0.5 & 0.75 & 1 \\ 0 & y_1^u & y_2^u & y_3^u & y_4^u & y_5^u \\ 1 & w_1^u & w_2^u & w_3^u & w_4^u & 1 \\ 0 & 0 & 0.25 & 0.5 & 0.75 & 1 \\ 0 & y_1^l & y_2^l & y_3^l & y_4^l & y_5^l \\ 1 & w_1^l & w_2^l & w_3^l & w_4^l & 1 \end{bmatrix} \tag{7}$$

These 18 remaining variables included in $\bar{\mathbf{A}}$ are shown in Fig. 1.

IV. Constructing Imitations

The parametric geometrical construction comprising the two NURBS curves, for which the parameters are defined by $\bar{\mathbf{A}}$, will form the starting point of our concise conceptual-level parametric airfoil. More specifically, we shall deploy its ability to approximate existing airfoils in the service of capturing knowledge about well-known supercritical airfoil shapes. Of course, what we have so far is, in itself, a parametric airfoil and, although it has too many parameters for conceptual design purposes, it is flexible enough to be capable of morphing into rather close imitations of a range of standard well-proven existing airfoils; it is this feature that we exploit in what follows.

For a selected range of classic airfoils, we seek sets of parameters for each, that, when plugged into the matrix $\bar{\mathbf{A}}$ that defines the NURBS airfoil, will approximate them to within as small a margin as possible. We use the overlapping areas to compute this margin. To be precise, we define the difference between a classic airfoil and its NURBS approximation as the sum of the areas *between the two airfoils* aligned such that their chords overlap, expressed as a percentage of the total area of the classic airfoil. Note that this is not the difference between the areas of the target and the approximation, as that could be near zero and the approximation could still snake undetected around the target airfoil, as long as the overshoots roughly cancel out the undershoots. Figure 2 illustrates a case of (exaggerated) snaking and highlights the area we are actually using as a difference metric.

We shall denote this difference by $d[\omega, \Omega(\bar{\mathbf{A}})]$, referring to the difference between some airfoil ω and a NURBS-based foil $\Omega(\bar{\mathbf{A}})$. With a difference metric in place, we can now formalize our notion of the best NURBS-based approximation of an existing airfoil.

Definition 1: $\Omega_\omega = \Omega(\bar{\mathbf{A}})$ is the NURBS imitation of the airfoil ω if

$$\forall\ \bar{\mathbf{A}}^* \neq \bar{\mathbf{A}}, \qquad d[\Omega(\bar{\mathbf{A}}), \omega] \leq d[\Omega(\bar{\mathbf{A}}^*), \omega]$$

Note that the minimization problem of Definition 1 and thus the finding of the NURBS imitation is usually not a trivial exercise, owing to the multimodal nature of the difference function d. The dimensionality of this landscape is also relatively high, as even the restricted $\bar{\mathbf{A}}$ has nine variables per surface. Thus, once a minimum has been found, however diligent we may have been in optimizing d, it is impossible to be absolutely certain that we have indeed located the global minimum. As a reminder of this, when using the notation introduced previously, we shall precede the name of the classic airfoil with the approximately equal symbol. For example, we shall use $\Omega_{\sim \mathrm{SC(2)\text{–}0714}}$ to refer to the best NURBS imitation of the NASA supercritical airfoil SC(2)–0714 we could find through a numerical optimization procedure.

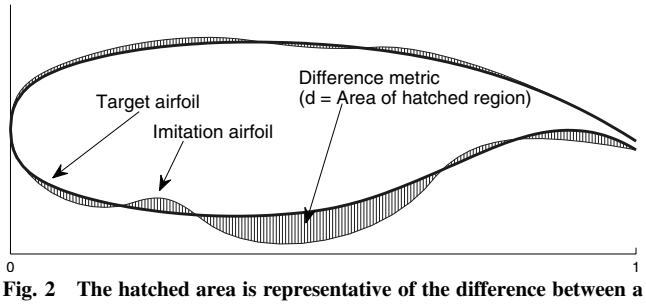

Fig. 2 The hatched area is representative of the difference between a target airfoil and its imitation. *d* is this area, expressed as a percentage of the area of the target airfoil (depicted here by the heavy black line contour).

As per criterion 4 of Sec. II, we shall focus on a range of supercritical airfoils. To begin with, let us consider eight well-known examples that we feel are representative of this class. What they all share is the goal that drove their conception, which is to maximize the drag-rise Mach number and thus maximize the cruising speed of an aircraft for which the wings are based on these sections. First, we have considered five of the NASA Phase 2 supercritical airfoils: the SC(2) family [13]. Three of these are the thin 6%-thickness-to-chord-ratio foils: SC(2)–0406, SC(2)–0606, and SC(2)–0706, designed for lift coefficients of 0.4, 0.6, and 0.7, respectively. The fourth is the much-studied SC(2)–0714 [22], and the final member of this group is the 18%-thick SC(2)–0518. Another high-thickness-to-chord-ratio airfoil we have included is the Dutch National Aerospace Laboratory NLR7301. It is slightly unusual among supercritical airfoils, not only by virtue of its 16.3% maximum thickness, but also because of its rather large nose radius. A 1975 paper by Boerstoel and Huizing [23] discusses in detail the hodograph calculations used in its design; the reader interested in detailed test results on it can find them, for example, in an extensive AGARD report [24]. The same report contains test data regarding the RAE2822, also included in our set. Finally, we use the RAE5215, featuring a thickness-to-chord ratio of 9.7%. It is the result of alterations made in the early 1970s to two earlier sections (RAE5213 and RAE5214), the chief aim of this development work being the elimination of rear separation at low Reynolds numbers [25].

We previously mentioned the challenges of optimizing the difference metric d. There is a broad range of optimizers that could be used to find the $\Omega_{\sim\omega}$s. We have experimented on the present set of functions with two potential candidates. First, a Nelder–Mead simplex pattern search was tested (see [26] for notes on the implementation used). Second, we considered a Broyden–Fletcher–Goldfarb–Shanno (BFGS) search (see, for example, [27]); this local quasi-Newton optimization procedure estimates the landscape gradients through finite differencing [these are needed, in turn, for the approximation of the Hessian $H(d)$]. Of the two, the BFGS required fewer evaluations of d in these tests, with a computing time of the order of tens of minutes on a standard desktop PC.

To reduce the size of the search space, we have set the values of the top and bottom ordinates of the trailing-edge points in the NURBS approximation (y_5^u and y_5^l, respectively) to those of the target classic airfoils we were attempting to imitate, thus cutting the dimensionality down to 16. To further simplify the search problem, we have implemented a two-stage approach. First, all weights were fixed at 1 and d was optimized subject to the control-point ordinates. The second, fine-tuning, stage then allowed the ordinates as well as the weights to vary.

Figure 3, a graphical depiction of the results of the search for the imitations of our eight chosen airfoils, shows these optimized sets of 16 numbers, as well as the corresponding difference values. Although these difference values give a good indication of the quality of these approximations, it is also revealing to consider the differences between target and clone in terms of their aerodynamic behavior. Considering, for example, NLR7301, Fig. 4 compares its pressure distribution against that of its NURBS imitation, computed using the Engineering Sciences Data Unit Viscous Garabedian–Korn (VGK) full-potential flow solver [28] for the flow conditions indicated on the diagram.

As a final note concerning the imitations, we have also determined them for the set of eight airfoils using $p = 3$ (fourth-order splines), but this did not offer considerable gains in flexibility and thus approximation accuracy (the results are shown in Table 1). In such circumstances, p is best kept to a minimum to reduce the computational overhead of evaluating additional layers of basis functions, unless the leading-edge curvature continuity enabled by fourth-order splines is specifically desired.

What these imitations show is that the definition of the two NURBS curves that make up the airfoil is flexible enough to provide good approximations of a fairly representative set of supercritical

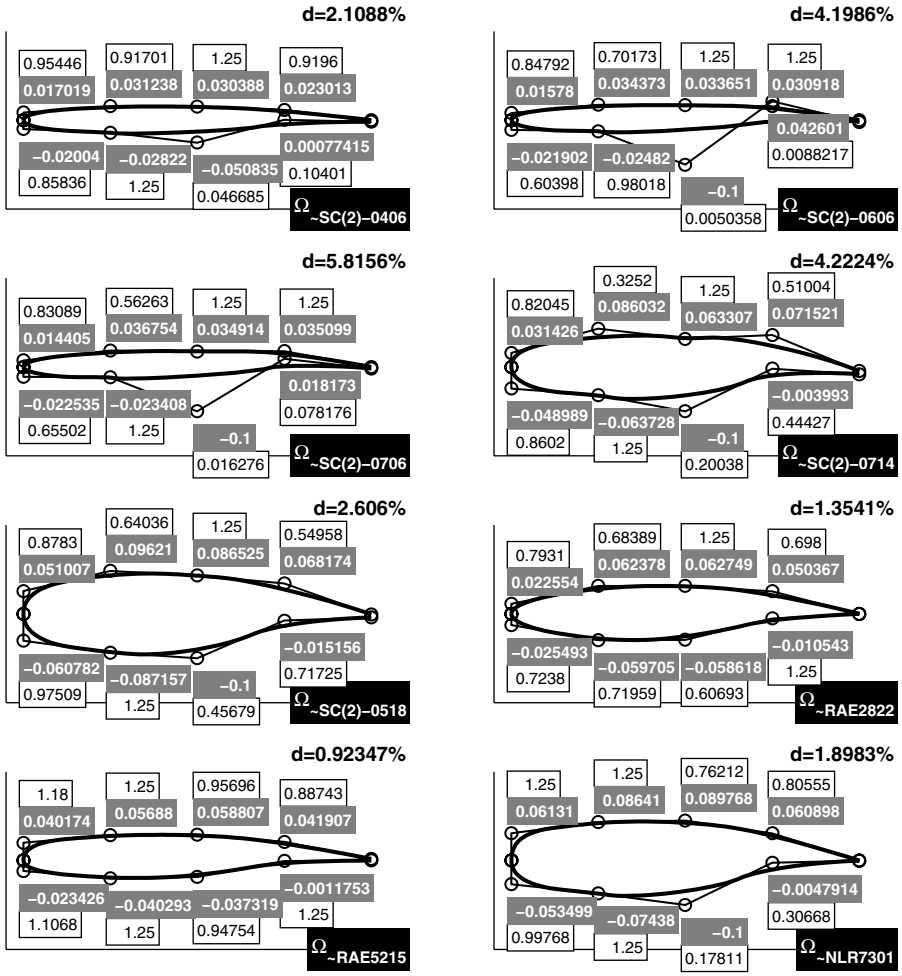

Fig. 3 NURBS imitations of eight classic airfoils and the differences d between them and their real counterparts. The axes are not to the same scale.

airfoils. We shall use these imitations (or, in the spirit of our introductory discussion in Sec. II, supercritical airfoil-likeness knowledge-capture devices) as the pillars of our parsimonious conceptual-level parameterization scheme, which we discuss next.

V. Linear Combinations and a Single-Variable Parameterization Scheme

In the Introduction we have underlined the importance of being parsimonious with the geometric parameterization of a conceptual airframe model and we made this our top priority. In that spirit, we shall now consider a NURBS-based formulation requiring a single slider control variable to sweep the span between two of the imitations we have prepared earlier. As we noted there, these imitations represent our knowledge (incomplete as it may be) of what makes a pair of NURBS a supercritical airfoil.

The essence of deploying this knowledge is simple: we reparameterize the matrix $\bar{\mathbf{A}}$ as the linear combination of two (imitations of) classics, with a weighting parameter α controlling the relative contributions of these two base airfoils. To formalize this, we define two new operators.

Definition 2: We define the binary operator $\star$ on the space of matrices of the form $\bar{\mathbf{A}}$, such that

$$\forall\ \alpha \in \mathrm{IR}{:}\alpha \star \bar{\mathbf{A}} = \Gamma_{\star}(\alpha) \bullet \bar{\mathbf{A}}$$

where $\bullet$ is the Haddamard (entrywise) matrix product and

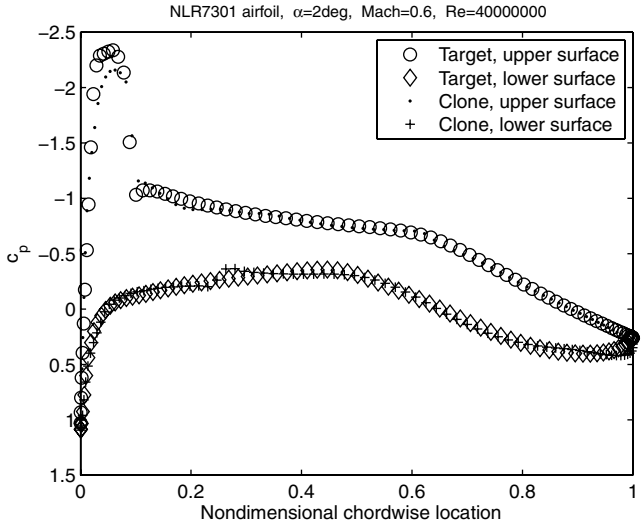

Fig. 4 Pressure profiles of NLR7301 and its NURBS imitation.

Table 1 The best difference metrics d obtained for the imitations of the eight classic airfoils using $p = 3$.

Airfoil	d
SC(2)–0406	1.8418%
SC(2)–0606	3.5542%
SC(2)–0706	5.7443%
SC(2)–0714	3.2509%
SC(2)–0518	2.2201%
RAE2822	0.83170%
RAE5215	0.9221%
NLR7301	2.2019%

$$\Gamma_\star(\alpha) = \begin{bmatrix} 1 & 1 & 1 & 1 & 1 & 1 \\ 1 & \alpha & \alpha & \alpha & \alpha & \alpha \\ 1 & \alpha & \alpha & \alpha & \alpha & 1 \\ 1 & 1 & 1 & 1 & 1 & 1 \\ 1 & \alpha & \alpha & \alpha & \alpha & \alpha \\ 1 & \alpha & \alpha & \alpha & \alpha & 1 \end{bmatrix} \tag{8}$$

Definition 3: We define the binary operator $\oplus$ on the space of matrices of the form $\bar{\mathbf{A}}$, such that

$$\forall\ \bar{\mathbf{A}}_1, \bar{\mathbf{A}}_2 : \bar{\mathbf{A}}_1 \oplus \bar{\mathbf{A}}_2 = \mathbf{A}_1 + \Gamma_\oplus \bullet \bar{\mathbf{A}}_2$$

where $\bullet$ is the Haddamard (entrywise) matrix product and

$$\Gamma_\oplus = \begin{bmatrix} 0 & 0 & 0 & 0 & 0 & 0 \\ 0 & 1 & 1 & 1 & 1 & 1 \\ 0 & 1 & 1 & 1 & 1 & 0 \\ 0 & 0 & 0 & 0 & 0 & 0 \\ 0 & 1 & 1 & 1 & 1 & 1 \\ 0 & 1 & 1 & 1 & 1 & 0 \end{bmatrix} \tag{9}$$

The matrices $\Gamma_\star(\alpha)$ and $\Gamma_\oplus$ are essentially stencils that control the elements of the generic parameterization that will be altered during the linear combination operation, which we define next.

Definition 4: Consider the NURBS imitations of some airfoils $\omega 1$ and $\omega 2$, denoted by $\Omega_{\omega 1} = \Omega(\bar{\mathbf{A}}_{\omega 1})$ and $\Omega_{\omega 2} = \Omega(\bar{\mathbf{A}}_{\omega 2})$, respectively (i.e., $\bar{\mathbf{A}}_{\omega 1}$ and $\bar{\mathbf{A}}_{\omega 2}$ contain the variables that define the two imitations). We shall refer to the single-variable parametric airfoil

$$\Omega_{\omega 1}^{\omega 2}(\alpha) = \Omega[\alpha \star \bar{\mathbf{A}}_{\omega 1} \oplus (1-\alpha) \star \bar{\mathbf{A}}_{\omega 2}]$$

where $\alpha \in [0, 1]$, as a linear combination NURBS airfoil over the bases $\omega 1$ and $\omega 2$.

The question arises now as to which bases $\omega 1$ and $\omega 2$ would ensure the best coverage of the design space as α sweeps its range. We have the eight imitations of Sec. IV to choose from; the question is how to measure the suitability of a given pair. As per criterion 4, for a given k, we aim to maximize the ability of the parametric airfoil to approximate existing supercritical sections. We can estimate this ability using the overlapping areas once again as the difference metric in the same way as we did with the imitations, by attempting to approximate a set of test sections that are representative of the supercritical family. In addition to the eight potential base sections, we have also included in this test set four more NASA phase 2 supercriticals for a better representation of the midrange of thickness-to-chord ratios: SC(2)–0410, SC(2)–0710, SC(2)–0412, and SC(2)–0712. We have evaluated the comparative abilities of the $C_8^2 = 28$ possible basis pairs to represent the 12 airfoils in this set. We have found the partnership of NLR7301 and SC(2)–0606 to work best. More formally, the evaluation of

$$\min\left\{\sum_{i=1}^{12} \min_\alpha d[\omega_i, \Omega_{\omega_{\text{base}1}}^{\omega_{\text{base}2}}(\alpha)] \,\middle|\, (\omega_{\text{base}1}, \omega_{\text{base}2}) \subset B\right\} \tag{10}$$

resulted in

$$(\omega_{\text{base}1}, \omega_{\text{base}2}) = (\text{NLR7301}, \text{SC(2)–0606})$$

where $\omega_1 = \text{SC(2)–0406}$ and

$$\omega_2 = \text{SC(2)–0606}, \ldots, \omega_{12} = \text{NLR7301}$$

are the test airfoils (see the legend of Fig. 5 for the full list) and

$$B = \{\text{SC(2)–0406}, \text{SC(2)–0606}, \ldots, \text{NLR7301}\}$$

is the list of the eight potential bases (as shown in Fig. 3).

This is not a particularly surprising outcome, as one would intuitively expect the process to yield one of the thinnest and one of the thickest airfoils as the best pillars, though it would have been harder to predict exactly which of the two thick and which of the three thin foils would provide the best supercritical airfoil-likeness knowledge representation. Approximating the 12 members of the test set with linear combinations of the chosen pair gave an average minimum difference of

$$\frac{1}{12}\sum_{i=1}^{12} \min_\alpha d[\omega_i, \Omega_{\sim\text{NLR7301}}^{\sim\text{SC(2)–0606}}(\alpha)] = 9.0601\% \tag{11}$$

This experiment is captured graphically in Fig. 5. The difference d curves corresponding to each test airfoil can be seen dipping, for an

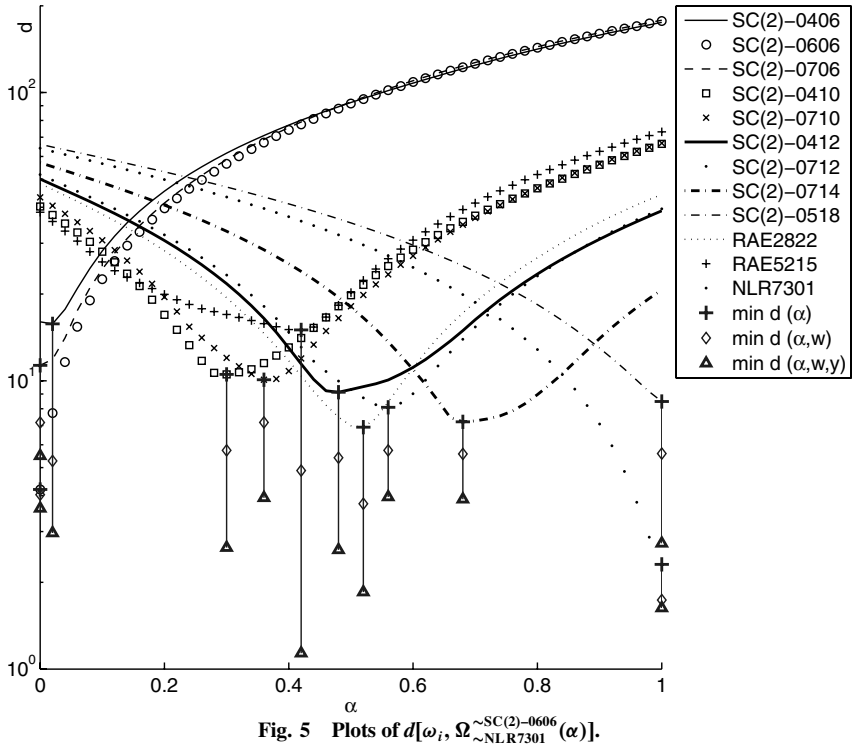

Fig. 5 Plots of $d[\omega_i, \Omega_{\sim\text{NLR7301}}^{\sim\text{SC(2)–0606}}(\alpha)]$.

optimum value of the linear combination factor α, to a minimum; this is the point at which the parametric airfoil

$$\Omega_{\sim\mathrm{NLR7301}}^{\sim\mathrm{SC(2)–0606}}(\alpha)$$

resembles the target (test) airfoil most closely. For example,

$$\Omega_{\sim\mathrm{NLR7301}}^{\sim\mathrm{SC(2)–0606}}(0.675) = \Omega[0.675 \star \bar{\mathbf{A}}_{\sim\mathrm{NLR7301}} \oplus 0.325 \star \bar{\mathbf{A}}_{\sim\mathrm{SC(2)–0606}}] \tag{12}$$

is the best approximation of SC(2)–0714 ($d = 7.1993$) that can be found using this scheme (we have run a direct search over the α domain with a resolution of 10^{-2} here; the curves show that there is little to be gained by employing a higher-resolution search).

It is worth emphasizing once more that, in the spirit of our list of requirements postulated in the introduction, we did not aim (and, indeed, cannot really hope) for extremely accurate approximations here. Instead, we are exploring the best that we can do with a single design variable available for controlling a parametric supercritical airfoil, while ensuring the satisfaction of the four other items of our Sec. II wish list.

Figure 5 is an illustration of the geometrical variations made possible by variations in the relative contributions of NLR7301 and SC(2)–0606 (controlled by α). For the aerodynamic impact of varying α, let us consider the following example. A target lift coefficient of $c_l = 0.6$ is required at a freestream Mach number of $M_\infty = 0.6$ and a Reynolds number of $Re = 3.5 \times 10^7$. A typical design study would trade c_d (directly related to fuel burn) versus thickness-to-chord ratio t/c, a measure of the structural efficiency of the design (the greater the thickness, the greater the maximum spar depth), and an indicator of the amount of fuel that can be carried in the wing. Figure 6 illustrates such a tradeoff for our example, depicting a Pareto front generated by sweeping the range of α, using the same VGK full-potential solver we employed in our earlier approximation accuracy comparison. We have highlighted the three nondominated designs, each representing a different blend of NLR7301 and SC(2)–0606.

Having established the basic mechanics of the geometrical operators we have introduced, let us now review the significance of the preceding discussion from the conceptual design standpoint, which is at the center of this paper.

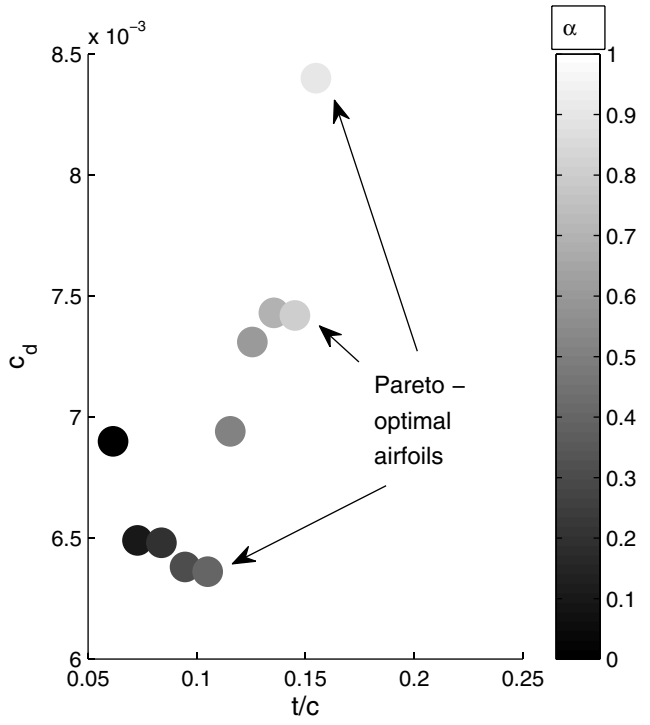

Fig. 6 Aerodynamics versus structures tradeoff study generated by sweeping the range of α.

VI. Designing with Linear Combination NURBS Airfoils

Let $v_1, v_2, \ldots, v_k$ be a set of design variables that define an airframe geometry. As we are focusing on airfoil definition here, let v_1 be the single parameter we are using to define: say, the wing root section. We do this as described previously by building a control polygon and a pair of NURBS curves (as depicted in Fig. 1), with the numbers needed to do this contained in the definition matrix, calculated in terms of the design variable v_1 as

$$\bar{\mathbf{A}} = v_1 \star \bar{\mathbf{A}}_{\sim\mathrm{NLR7301}} \oplus (1 - v_1) \star \bar{\mathbf{A}}_{\sim\mathrm{SC(2)–0606}} \tag{13}$$

For convenience, we split the airframe description into the airfoil thus defined,

$$\Omega_{\sim\mathrm{NLR7301}}^{\sim\mathrm{SC(2)–0606}}(v_1)$$

and $G(v_2, v_3, \ldots, v_k)$, the latter denoting the rest of the geometry.

Consider now the functional

$$\mathcal{F}[\Omega_{\sim\mathrm{NLR7301}}^{\sim\mathrm{SC(2)–0606}}(v_1), G(v_2, v_3, \ldots, v_k)]$$

mapping some figure of merit to the airframe geometry. Typically, this is an objective (computed through a numerical simulation), which we seek to maximize or minimize. An example is total airframe drag at the angle of attack at which the total lift equals the all-up weight. Thus, the conceptual design search can be summarized as the minimization problem

$$\min_{v_1 \in [0,1], v_2, \ldots, v_k} \mathcal{F}[\Omega_{\sim\mathrm{NLR7301}}^{\sim\mathrm{SC(2)–0606}}(v_1), G(v_2, v_3, \ldots, v_k)] \tag{14}$$

to which the dimensionality of the airfoil only contributes one.

The linear combination NURBS airfoil essentially represents a continuum of supercritical airfoils between the two bases, the imitations of which it reproduces exactly at the extreme values of v_1 (NLR7301 at $v_1 = 1$ and SC(2)–0606 at $v_1 = 0$). Therefore, the optimization problem (14) can be solved with any continuous variable optimization algorithm. As an aside, the same geometric construction can be used for a search over a given catalog of imitations, rather than over the continuum bridging the gap between two imitations. For example, if we take the set B of our eight imitated classic airfoils (those shown in Fig. 3) as the catalog, the problem can be recast as

$$\min_{v_1 \in \{1,2,\ldots,8\}, v_2, \ldots, v_k} \mathcal{F}[\Omega_{\sim B(v_1)}, G(v_2, v_3, \ldots, v_k)] \tag{15}$$

which means that the search will now be discrete-valued along the dimension v_1.

Returning now briefly to Fig. 5, earlier we left unexplained part of the experiment depicted therein, and this is the appropriate moment to return to it. For every test airfoil, once we established the weighting that brings the parametric linear combination NURBS airfoil nearest to it, we froze the weighting at that value and further minimized the difference d using a Nelder–Mead simplex pattern search, this time subject to the control-point weights. The optima of these eight-dimensional local search processes can be read off the chart as the ordinates of the diamond symbols (note that these are not the globally best approximations that can be obtained for the various test airfoils, merely the minima of the local basins of attraction). Next, we ran the Nelder–Mead search once more, this time allowing both the weights and the control-point ordinates to vary, giving the minima for which the difference values are the ordinates of the triangle symbols.

This logic could also be applied to the optimization of $\mathcal{F}$ at the later stages of the development process, perhaps as a preliminary design operation, in which we are willing to trade increased dimensionality for potentially better objective functional values. Defining the stencil matrix

Table 2 The differences between the test set of 12 airfoils and the closest linear combination NURBS airfoils over the bases RAE5215, SC(2)–0518, and SC(2)–0606, obtained by minimizing d subject to α_1,α_2 and α_3 (where $\alpha_1 + \alpha_2 + \alpha_3 = 1$).

ω	α_1	α_2	α_3	$d[\omega_{\sim\text{RAE5215}}\Omega^{\sim\text{SC(2)–0606}}_{\sim\text{SC(2)–0518}}(\alpha_1,\alpha_2,\alpha_3)]$
SC(2)–0406	0.0042	0	0.9958	12.3886%
SC(2)–0606	0	0	1	4.1986%
SC(2)–0706	0	0	1	11.3089%
SC(2)–0410	0	0.2669	0.7331	9.1881%
SC(2)–0710	0.7072	0.0930	0.1997	10.7707%
SC(2)–0412	0	0.4496	0.5504	6.7767%
SC(2)–0712	0.6030	0.3121	0.0849	8.0071%
SC(2)–0714	0.1237	0.5962	0.2801	4.6457%
SC(2)–0518	0	1	0	2.6060%
RAE2822	0.5172	0.3002	0.1826	7.5347%
RAE5215	1	0	0	0.9235%
NLR7301	0.2155	0.7845	0	6.0293%

$$\Gamma_w = \begin{bmatrix} 0 & 0 & 0 & 0 & 0 & 0 \\ 0 & 0 & 0 & 0 & 0 & 0 \\ 0 & 1 & 1 & 1 & 1 & 0 \\ 0 & 0 & 0 & 0 & 0 & 0 \\ 0 & 0 & 0 & 0 & 0 & 0 \\ 0 & 1 & 1 & 1 & 1 & 0 \end{bmatrix} \tag{16}$$

we can formalize this operation as

$$\min_{\Gamma_w \bullet \bar{\mathbf{A}}, v_2, \ldots, v_k} \mathcal{F}[\Omega^{\sim\text{SC(2)–0606}}_{\sim\text{NLR7301}}(v_1^{\text{opt}}), G(v_2, v_3, \ldots, v_k)] \tag{17}$$

where we have frozen v_1 at v_1^{opt}, the optimum value found during the conceptual design process, and we are now allowing the control-point weights to be subjected to the optimization process. Finally, mirroring the experiments of Fig. 5 in a real design optimization context, we can now turn on all of the degrees of freedom built into our NURBS airfoil definition by allowing every entry in $\bar{\mathbf{A}}$ to vary in an optimization process that can be summarized as

$$\min_{\bar{\mathbf{A}}, v_2, \ldots, v_k} \mathcal{F}[\Omega^{\sim\text{SC(2)–0606}}_{\sim\text{NLR7301}}(v_1^{\text{opt}}), G(v_2, v_3, \ldots, v_k)] \tag{18}$$

At this level, the formulation proposed here becomes very similar to those described by Lépine et al. [8] and Painchaud-Ouellet et al. [9]. In terms of meeting our initial criteria listed in Sec. II, the last two preliminary-design-type steps now have increasing dimensionalities, which are hard to justify against criterion 1.[‡] Also, they depart from the third criterion of our wish list, as the parameterization can now yield unphysical shapes too (although these are fairly unlikely to occur, as an aerodynamics-based $\mathcal{F}$ will probably still favor smooth reasonable shapes). We have, however, used the same geometrical entities for these different levels of optimization (criterion 5), by merely varying the method whereby the control-point weights and ordinates are calculated. In other words, the same model can be used throughout the entire design process, offering potential benefits in terms of development cost reduction.

Let us now return to the pure linear combination approach by considering the possibility of incorporating additional knowledge into the parametric foil, simply by using additional learning cases.

VII. Learning from More Examples

Let us consider the potential flexibility enhancements that additional base airfoils (as further learning examples) would allow us. To this end, it is fairly straightforward to conceive an extension of Definition 4, as follows.

[‡]This increase in dimensionality is the principal reason behind limiting the number of control points to six here. Although the dimensionality of the search across the space of linear combinations is independent of the number of control points, these subsequent steps can easily become quite expensive if the number of control points is large. Conversely, fewer than six control points, in our experience, yields inaccurate learning of the test cases.

Definition 5: Consider the NURBS imitations of airfoils $\omega1$, $\omega2$, $\omega3$, and $\omega4$, denoted by $\Omega_{\omega1} = \Omega(\bar{\mathbf{A}}_{\omega1})$, $\Omega_{\omega2} = \Omega(\bar{\mathbf{A}}_{\omega2})$, $\Omega_{\omega3} = \Omega(\bar{\mathbf{A}}_{\omega3})$, and $\Omega_{\omega4} = \Omega(\bar{\mathbf{A}}_{\omega4})$, respectively (i.e., $\bar{\mathbf{A}}_{\omega1}$, $\bar{\mathbf{A}}_{\omega2}$, $\bar{\mathbf{A}}_{\omega3}$, and $\bar{\mathbf{A}}_{\omega4}$ contain the variables that define the four imitations). We shall refer to the parametric airfoil

$$_{\omega1}\Omega^{\omega3}_{\omega2}(\alpha_1,\alpha_2,\alpha_3) = \Omega[\alpha_1 \star \bar{\mathbf{A}}_{\omega1} \oplus \alpha_2 \star \bar{\mathbf{A}}_{\omega2} \oplus \alpha_3 \star \bar{\mathbf{A}}_{\omega3}]$$

where α_1, α_2, $\alpha_3 \in \text{IR}^+$, and $\alpha_1 + \alpha_2 + \alpha_3 = 1$ as a linear combination NURBS airfoil over the bases $\omega1$,$\omega2$, and $\omega3$ and to the parametric airfoil

$$\begin{aligned} &^{\omega4}_{\omega1}\Omega^{\omega3}_{\omega2}(\alpha_1,\alpha_2,\alpha_3,\alpha_4) \\ &\quad = \Omega[\alpha_1 \star \bar{\mathbf{A}}_{\omega1} \oplus \alpha_2 \star \bar{\mathbf{A}}_{\omega2} \oplus \alpha_3 \star \bar{\mathbf{A}}_{\omega3} \oplus \alpha_4 \star \bar{\mathbf{A}}_{\omega4}] \end{aligned}$$

where $\alpha_1, \alpha_2, \alpha_3, \alpha_4 \in \text{IR}^+$, and $\alpha_1 + \alpha_2 + \alpha_3 + \alpha_4 = 1$ as a linear combination NURBS airfoil over the bases $\omega1$, $\omega2$, $\omega3$, and $\omega4$.

The problem of approximating a given target airfoil with a linear combination NURBS airfoil over three bases is virtually the same as with two bases. The only exception is that the optimization problem is now subject to three α instead of one. The overall dimensionality is reduced from three to two by the additional equality constraint, though in most cases, from a computational implementation standpoint, the problem is more readily viewed as three-dimensional and constrained, rather than projected onto the two-dimensional plane $\alpha_1 + \alpha_2 + \alpha_3 = 1$ (α_1, α_2, and $\alpha_3 \in \text{IR}^+$) and unconstrained (see the homomorphous mapping approach of Monson and Seppi [29] for taking the latter route, if preferred).

Once again, we need to select the bases that, with their α optimized, best approximate the other members of our representative set of 12 test airfoils (this being a simple test of the satisfaction of criterion 4). Formally, we are seeking the solution of the two-level minimization problem:

$$\begin{aligned} \min \Bigg\{ &\sum_{i=1}^{12} \min_{\alpha_1,\alpha_2,\alpha_3} d[\omega_i, \omega_{\text{base1}}\, \Omega^{\omega_{\text{base3}}}_{\omega_{\text{base2}}}(\alpha_1,\alpha_2,\alpha_3)] \\ &\times \Big| (\omega_{\text{base1}}, \omega_{\text{base2}}, \omega_{\text{base3}}) \subset B \Bigg\} \end{aligned} \tag{19}$$

where all $C_8^3 = 56$ subsets of three of the set of eight potential base airfoils are tested across the set of 12 test airfoils. A direct search solve of Eq. (19) yielded

$$(\omega_{\text{base1}}, \omega_{\text{base2}}, \omega_{\text{base3}}) = (\text{RAE5215}, \text{SC(2)–0518}, \text{SC(2)–0606})$$

with the difference metric averaging 7.0315% over the 12 target sections, which is around three-fourths of the estimated average approximation error of the two basis airfoil scheme (9.0601%). To single out one particular example, the difference metric between SC(2)–0714 and its best approximation was found to be

Table 3 The differences between the test set of 12 airfoils and the closest linear combination NURBS airfoils over the bases RAE5215, SC(2)–0518, SC(2)–0706, and SC(2)–0406 obtained by minimizing d subject to α_1, α_2, α_3 and α_4 (where $\alpha_1 + \alpha_2 + \alpha_3 + \alpha_4 = 1$).

ω	α_1	α_2	α_3	α_4	$d\left[\omega_{\sim\text{RAE5215}}^{\sim\text{SC(2)–0406}}\Omega_{\sim\text{SC(2)–0518}}^{\sim\text{SC(2)–0706}}(\alpha_1,\alpha_2,\alpha_3,\alpha_4)\right]$
SC(2)–0406	0	0	0	1	2.1088%
SC(2)–0606	0	0	0.8886	0.1114	5.8129%
SC(2)–0706	0	0	1	0	5.8156%
SC(2)–0410	0	0.2968	0.1673	0.5359	4.0453%
SC(2)–0710	0.6250	0.1250	0.1250	0.1250	10.5663%
SC(2)–0412	0	0.4691	0.1431	0.3877	3.5596%
SC(2)–0712	0.5464	0.3378	0.0032	0.1124	7.9753%
SC(2)–0714	0.0245	0.6323	0.1302	0.2130	3.8678%
SC(2)–0518	0	1	0	0	2.6060%
RAE2822	0.4240	0.3417	0.0964	0.1380	6.8773%
RAE5215	1	0	0	0	0.9235%
NLR7301	0.2155	0.7845	0	0	6.0055%

$$
\begin{aligned}
&d[\text{SC(2)–0714}_{\sim\text{RAE5215}}\Omega_{\sim\text{SC(2)–0518}}^{\sim\text{SC(2)–0606}}(0.1237, 0.5962, 0.2801)]\\
&\quad = d[\text{SC(2)–0714}, \Omega(0.1237 \star \bar{\mathbf{A}}_{\sim\text{RAE5215}} \oplus 0.5962\\
&\qquad \star \bar{\mathbf{A}}_{\sim\text{SC(2)–0518}} \oplus 0.2801 \star \bar{\mathbf{A}}_{\sim\text{SC(2)–0606}})]\\
&\quad = 4.6457\%
\end{aligned}
$$

approximately two-thirds of the difference metric value of the two basis approximation of SC(2)–0714 [see Eq. (12)]. Table 2 contains the full results of this experiment. Repeating the exercise for four bases, we seek the solution of the two-level minimization problem:

$$
\begin{aligned}
\min\Bigg\{&\sum_{i=1}^{12} \min_{\alpha_1,\alpha_2,\alpha_3,\alpha_4} d[\omega_i, {}^{\omega_{\text{base4}}}_{\omega_{\text{base1}}}\Omega^{\omega_{\text{base3}}}_{\omega_{\text{base2}}}(\alpha_1,\alpha_2,\alpha_3,\alpha_4)]\\
&\times \Big|(\omega_{\text{base1}}, \omega_{\text{base2}}, \omega_{\text{base3}}, \omega_{\text{base4}}) \subset B\Bigg\} \qquad (20)
\end{aligned}
$$

where the $C_8^4 = 70$ subsets of four of the set of eight potential base airfoils are now evaluated as potential bases over the set of 12 test airfoils. From a direct search solve of Eq. (19) results

$$
\begin{aligned}
&(\omega_{\text{base1}}, \omega_{\text{base2}}, \omega_{\text{base3}}, \omega_{\text{base4}})\\
&\quad = (\text{RAE5215}, \text{SC(2)–0518}, \text{SC(2)–0706}, \text{SC(2)–0406})
\end{aligned}
$$

with the averaged difference metric now dropping to 4.9874%. Comparing this with the best we could achieve with only two basis airfoils (almost twice this difference metric value: 9.0601%) confirms the increase in the amount of additional geometrical features incorporated into the knowledge base of the parametric airfoil. Table 3 contains the full results of this experiment.

VIII. Conclusions

We have looked at extremely concise NURBS-based parametric airfoil formulations, including one in which the sole variable controls the relative contributions of two base sections to the parameterized shape. This is based on a fairly general technique, which we have demonstrated as being able to capture the salient features of a family of shapes.

More refined studies across a broader design space are possible by learning from further examples; we have shown this too on our chosen family of airfoils. The results indicated that adding one or two additional sections into the linear combination increases the flexibility (and thus design space coverage) of the parametric airfoil. Further, we have demonstrated that the same geometrical setup used in the linear combination scheme can be recycled for preliminary design studies, in which, if we sacrifice parsimony, extra flexibility is available for local optimization purposes, without the need for rebuilding the model.

The general thrust of the approach described here can be adapted for other types of geometry, including NURBS surfaces. For instance, it would be possible to capture knowledge on existing airliner fuselage shapes by wrapping a NURBS control mesh around them and using a similar approach to employ this knowledge to populate the design space defined by the example fuselages. We envisage this type of approach being particularly suited to the concise parameterization of very complex shapes, as it is a simple way of reducing dimensionality using case-based knowledge about what constitutes a reasonable shape.

Acknowledgments

The author would like to thank the Royal Academy of Engineering and the Engineering and Physical Sciences Research Council (EPSRC) for the financial support of this work through their Research Fellowship program.

References

[1] McKay, M., Conover, W., and Beckman, R., "A Comparison of Three Methods for Selecting Values of Input Variables in the Analysis of Output from a Computer Code," *Technometrics*, Vol. 21, No. 2, 1979, pp. 239–245. doi:10.2307/1268522

[2] Jameson, A., "Aerodynamic Design via Control Theory," *Journal of Scientific Computing*, Vol. 3, No. 3, 1988, pp. 233–260. doi:10.1007/BF01061285

[3] Jameson, A., "Optimum Aerodynamic Design Using Control Theory," *Computational Fluid Dynamics Review*, M. Hafez, and K. Oshima, (eds.), Wiley, New York, 1995.

[4] Giammichele, N., Trépanier, J.-Y., and Tribes, C., "Airfoil Generation and Optimization Using Multiresolution B-Spline Control with Geometrical Constraints," AIAA Paper 2007-1916, 2007.

[5] Hicks, R. M., and Henne, P. A., "Wing Design by Numerical Optimization," *Journal of Aircraft*, Vol. 15, No. 7, 1978, pp. 407–412. doi:10.2514/3.58379

[6] Reuther, J., Jameson, A., Alonso, J. J., Remlinger, M. J., and Saunders, D., "Constrained Multipoint Aerodynamic Shape Optimization Using an Adjoint Formulation and Parallel Computers," *Journal of Aircraft*, Vol. 36, No. 1, 1999, pp. 61–74. doi:10.2514/2.2414

[7] Kulfan, B. M., "Universal Parametric Geometry Representation Method," *Journal of Aircraft*, Vol. 45, No. 1, 2008, pp. 142–158. doi:10.2514/1.29958

[8] Lépine, J., Guibault, F., Trépanier, J.-Y, and Pépin, F., "Optimized Nonuniform Rational B-Spline Geometrical Representation for Aerodynamic Design of Wings," *AIAA Journal*, Vol. 39, No. 11, 2001, pp. 2033–2041. doi:10.2514/2.1206

[9] Painchaud-Ouellet, S., Tribes, C., Trépanier, J.-Y., and Pelletier, D., "Airfoil Shape Optimization Using a Nonuniform Rational B-Splines Parameterization Under Thickness Constraint," *AIAA Journal*, Vol. 44, No. 10, 2006, pp. 2170–2178. doi:10.2514/1.15117

[10] Sobieczky, H., "Parametric Airfoils and Wings," *Notes on Numerical Fluid Mechanics*, Vol. 68, 1998, pp. 71–88.
[11] Sóbester, A., and Barrett, T., "The Quest for a Truly Parsimonious Airfoil Parameterization Scheme," AIAA Paper 2008-8879, 2008, pp. 1–23.
[12] Robinson, G. M., and Keane, A. J., "Concise Orthogonal Representation of Supercritical Airfoils," *Journal of Aircraft*, Vol. 38, No. 3, 2001, pp. 580–583.
doi:10.2514/2.2803
[13] Harris, C. D., "NASA Supercritical Airfoils: A Matrix of Family-Related Airfoils," NASA, TP 2969, 1990.
[14] Vanderplaats, G. N., *Numerical Optimization techniques for Engineering Design: With Applications*, McGraw–Hill, New York, 1984.
[15] Collins, L., and Saunders, D., "Profile: Airfoil Geometry Manipulation and Display," NASA CR 177332, 1997.
[16] Versprille, K. J., "Computer-Aided Design Applications of the Rational B-Spline Approximation Form," Ph.D. Thesis, Syracuse Univ., Syracuse, NY, 1975.
[17] Schramm, U., Pilkey, W. D., DeVries, R. I., and Zebrowski, M. P., "Shape Design for Thin-Walled Beam Cross Sections Using Rational B-Splines," *AIAA Journal*, Vol. 33, No. 11, 1995, pp. 2205–2211.
doi:10.2514/3.12870
[18] Samareh, J. A., "Novel Multidisciplinary Shape Parameterization Approach," *Journal of Aircraft*, Vol. 38, No. 6, 2001, pp. 1015–1024.
doi:10.2514/2.2888
[19] Cox, M. G., "The Numerical Evaluation of B-Splines," *Journal of the Institute of Mathematics and Its Applications*, Vol. 10, No. 2, 1972, pp. 134–149.
[20] De Boor, C., "On Calculating with B-splines," *Journal of Approximation Theory*, Vol. 6, No. 1, 1972, pp. 50–62.
doi:10.1016/0021-9045(72)90080-9
[21] Piegl, L., and Tiller, W., *The NURBS Book*, Springer–Verlag, Heidelberg, 1997.
[22] Jenkins, R. V., Hill, A. S., and Ray, E. J., "Aerodynamic Performance and pressure Distributions for a NASA SC(2)–0714 Airfoil Tested in the Langley 0.3-Meter Transonic Cryogenic Tunnel," NASA Langley Research Center, TM-4044, Hampton, VA, 1988.
[23] Boerstoel, J. W., and Huizing, G. H., "Transonic Shock-Free Aerofoil Design by an Analytic Hodograph Method," *Journal of Aircraft*, Vol. 12, No. 9, 1975, pp. 730–736.
doi:10.2514/3.59864
[24] "Experimental Data Base for Computer Program Assessment—Report of the Fluid Dynamics Panel Working Group 04," AGARD Rept. AR-138, Neuilly-sur-Seine, France, 1979.
[25] Wilby, P. G., "The Design and Aerodynamic Characteristics of the RAE 5215 Aerofoil," Aeronautical Research Council, Paper 1386, 1974.
[26] Lagarias, J., Reeds, J. A., Wright, M. H., and Wright, P. E., "Convergence Properties of the Nelder-Mead Simplex Method in Low Dimensions," *SIAM Journal on Optimization*, Vol. 9, No. 1, 1998, pp. 112–147.
doi:10.1137/S1052623496303470
[27] Broyden, C. G., "The Convergence of a Class of Double-Rank Minimization Algorithms," *Journal of the Institute of Mathematics and Its Applications*, Vol. 6, No. 3, 1970, pp. 76–90.
[28] Freestone, M. M., "Transonic Data Memorandum: VGK Method for Two-Dimensional Aerofoil Sections," ESDU International, Rept. 96028, London, Oct. 1996.
[29] Monson, C. K., and Seppi, K. D., "Linear Equality Constraints and Homomorphous Mappings in PSO," *Proceedings of the Congress on Evolutionary Computation*, Inst. of Electrical and Electronics Engineers, Piscataway, NJ, 2005, pp. 73–80.

J. Samareh
Associate Editor